Title

Observational Evidence of Strong Forcing from Aerosol Effect on Low Cloud Coverage

Authors

Tianle Yuan[1,2,*], Hua Song[2,3], Robert Wood[4], Lazaros Oreopoulos[2], Steven Platnick[2], Chenxi Wang[1,2], Hongbin Yu[2], Kerry Meyer[2], Eric Wilcox[5]

Affiliations

[1]Joint Center for Earth Systems Technology, University of Maryland, Baltimore County
[2]Sciences and Exploration Directorate, Goddard Space Flight Center
[3]SSAI, Inc.
[4]Department of Atmospheric Sciences, University of Washington
[5]Desert Research Institute

[*]Corresponding author: tianle.yuan@nasa.gov

Abstract

Aerosols cool the Earth's climate indirectly by increasing low cloud brightness and their coverage (Cf), constituting the aerosol indirect forcing (AIF). The forcing partially offsets the greenhouse warming and positively correlates with the climate sensitivity. However, it remains highly uncertain. Here we show direct observational evidence for strong forcing from Cf adjustment to increased aerosols and weak forcing from cloud liquid water path adjustment. We estimate that the Cf adjustment drives between 52% and 300% of additional forcing to the Twomey effect over the ocean and a total AIF of -1.1 ± 0.8 Wm^{-2}. The Cf adjustment follows a power law as function of background cloud droplet number concentration, N_d. It thus depends on time and location and is stronger when N_d is low. Cf only increases substantially when background clouds start to drizzle, suggesting a role for aerosol-precipitation interactions. Our findings highlight the Cf adjustment as the key process for reducing the uncertainty of AIF and thus future climate projections.

MAIN TEXT

1. Introduction

Tiny airborne particles – aerosols – can affect the energy balance of the Earth's climate by modifying cloud brightness and coverage(*1*, *2*). The resulting energy balance perturbation constitutes a radiative forcing, known as the aerosol indirect forcing. It partially offsets the positive forcing due to greenhouse gases. Given the observed global temperature increase and positive forcing from greenhouse gases, strong negative aerosol indirect forcing implies a high climate sensitivity because the observed warming would have been a result of a small net positive forcing(*3*). The total aerosol indirect forcing is estimated to be between -1.7 and -0.3

Wm^{-2} based on observations and represents the largest source of uncertainty in our forcing estimates(*3*). The uncertainty range – $1.4Wm^{-2}$ – is about half of the historic forcing from greenhouse gases and leads to considerable uncertainty in climate sensitivity estimated using historic data, which has important implications for climate adaptation and mitigation plans(*4*).

Marine low clouds are the largest contributor to reflecting solar radiation back to space and aerosol effects on them contribute substantially to the total aerosol indirect forcing. The fraction of reflected solar radiation is largely determined by three cloud parameters of marine low clouds: liquid water path (LWP), cloud droplet number concentration (N_d), and cloud coverage (Cf). Aerosols can modify all three through changing N_d. Increasing aerosol concentration leads to higher N_d and smaller cloud droplet effective size (R_e), which makes marine low clouds brighter if LWP and Cf remain constant, the so-called Twomey effect(*1*). The Twomey effect is widely supported by observational evidence. But LWP and Cf do adjust to changes in N_d and R_e. The decreased R_e from increasing N_d can delay and suppress precipitation formation by suppressing the droplet collision-coalescence process. Suppressed precipitation in turn can increase LWP and Cf by reducing the cloud water sink and help clouds to live longer(*2*). However, other physical processes can work against this chain reaction(*5*, *6*). For example, smaller and more numerous droplets can introduce stronger evaporation when mixed with dry environmental air, thus increasing the cloud water sink to the ambient air and decreasing LWP and Cf(*5*). Such processes form complex feedback loops in the cloud system that give rise to the final LWP and Cf adjustments. A key unknown is how much additional forcing is introduced by these adjustments in addition to the Twomey effect.

Global satellite observations can provide empirical estimates on these adjustments(*3*, *7*). There is growing evidence that the LWP adjustment can be bidirectional and depends on the background conditions(*8–10*). Existing evidence for Cf adjustment is more limited and less well-quantified, which manifests in a wide uncertainty range in the forcing due to Cf adjustment(*3*, *7*), despite clear evidence of Cf increase in response to ship-emitted aerosols in case studies(*11*, *12*). Some studies use correlation and covariance between satellite observed LWP and Cf and aerosol loading, but their results can be affected by retrieval biases of aerosols and clouds, aerosol swelling with humidity, unresolved vertical profiles of aerosols and clouds(*13*), removal by precipitation, among other possible confounding correlations(*3*). Other studies instead analyze the covariance using derived N_d, instead of aerosol loading, to alleviate aerosol retrieval bias complications and still find contrasting responses of LWP to N_d and increasing Cf to N_d(*14–16*). But retrieval artifacts and potential confounding correlations still exist. For example, derived N_d is biased low for broken and low-Cf clouds and the positive correlation between N_d and Cf can at least partially be attributed to this bias(*3*, *17*). Such relationships remain correlational and do not constitute causality, which introduces uncertainty in attributing and quantifying the forcing due to the LWP and Cf adjustments.

Here we directly measure the cloud LWP and Cf adjustments attributable to aerosol influences by contrasting polluted clouds in ship-tracks with nearby background clouds, overcoming the limitation of correlation studies. Our main goal is to quantify the ratio of contributions of the LWP and Cf adjustments to the total aerosol indirect forcing compared to that of the Twomey effect (e.g., *10)*. We use ship-tracks as our 'opportunistic experiments' (*10*, *18*), where the LWP and Cf adjustments can be attributed to ship-emitted aerosols, to avoid the covariance between LWP and Cf and N_d that are driven by meteorology and other confounding factors(*18*) (Figure 1). Previous analyses of ship-tracks and similar opportunistic experiments suggest variable LWP adjustments to aerosols(*10*, *19–21*). Toll et al.(*10*) show a slight LWP increase in ship-tracks on average and the magnitude partially results from the balance

between entrainment drying and moistening by precipitation suppression. The Cf adjustment, though clearly observed and modeled(*22–24*) in case studies, has not been systematically quantified using ship-track observations and remains highly uncertain(*3*, *7*). We assemble a large collection of ship-track samples and analyze the LWP and Cf adjustments with them to address the knowledge gap.

2. Results

2.1 Ship-track sampling and mean cloud response

We previously developed an algorithms to automatically detect ship-tracks globally in the Aqua Moderate Resolution Imaging Spectrometer (MODIS) data and produce ship-track masks that include pixels polluted by ship-emitted aerosols(*25*, *26*) (Figure 1 and Figures S1&2 in Method). Here we use ship-tracks derived from the algorithm. A separate analysis algorithm finds surrounding background cloud pixels with a width of 20 MODIS pixels, equivalent to around 20km (see Method). We contrast the properties of polluted and background low clouds using MODIS retrievals within individual 128pixel x 128pixel blocks (see Method section for details). We choose the size of 128pixel x 128pixel in order to have sufficient pixel counts in a block to obtain accurate estimate of cloud fractions in both ship-track and control clouds. In total, we find 295,036 blocks with ship-tracks in 18 years of Aqua MODIS record (Figure 2 and Method). Our total number of ship-track pixels is equivalent to around 12 million ship-track segments as defined in Toll et al.(*10*) assuming an average ship-track width of 10pixels, representing an increase of several orders of magnitudes in the number of samples. Our samples include ship-tracks of many different sizes and thus ages.

The ship-track samples cover wide range of meteorology and background cloud conditions over the global ocean (Figure S3). Nearly all ship-tracks occur in a relatively stable environment with the estimated inversion strength(*27*) greater than 0 K. Cloud top height of our samples has a wide range between a few hundred meters and a couple of kilometers with a peak at around 800m. Above cloud top relative humidity ranges between 10% to 90% and its distribution has two local maxima at 10% and 90%. Background N_d ranges from a few droplets cm^{-3} to a few hundred cm^{-3} with a strong peak at the low end. We include most ship-track samples in our analysis, recognizing that ship-track detectability has a wide range(*23*) and implicit sampling bias can be introduced by imposing filters (see discussion in Method section and Figures S4&5). Indeed, notable changes in probability distribution functions (PDFs) of background cloud properties occur when samples are filtered using different criteria (Figure S4). On average, we measure a reduction of 2.9 μm in R_e, and increases of 5.8 g/m^2, and 9 % in LWP and Cf in polluted clouds within ship-tracks compared to the background clouds (Figure 3). The standard deviations of such changes are 2 μm, 44 g/m^2, and 19%, respectively. They are much larger than the mean change for the LWP and Cf, highlighting strong variability in the adjustments of these variables.

2.2 Cf and LWP adjustments and the role of background conditions

The Cf adjustment to additional aerosols is a positive and non-linear function of background N_d or R_e (Figure 4). The mean absolute Cf increase in all ship-track samples is 9%. We note that the mean value is a simple average and does not account for occurrence frequency of background cloud conditions, which is addressed when we later calculate radiative effect from Cf adjustment. Our method allows for bidirectional Cf adjustments, but only in a small percentage of cases, Cf adjustment is negative (Figure 3). Small average Cf increases (1~2%) are observed in clouds where mean R_e is smaller than 14 μm, or mean N_d greater than 60 cm^{-3}.

Once background clouds are cleaner than the threshold, i.e., N_d less than 60 cm^{-3} or mean R_e greater than around 14 μm, the sensitivity of Cf to N_d, dCf/dN_d, increases substantially with decreasing background N_d, or increasing R_e. Our results agree with similar N_d threshold behavior previously reported using different approaches and data (*21*). The 14μm threshold is physically meaningful since low clouds start to produce substantial drizzle that depletes cloud water once R_e exceeds the 14 μm threshold (*28*). Further increase in R_e and thus precipitation rate can quickly deplete cloud water and reduce Cf. Our measurements indicate that the Cf increase due to aerosols only becomes substantial under such background cloud conditions, likely through precipitation suppression, which supports the conceptual mechanism proposed by Albrecht (*2*).

Moreover, Cf increase due to aerosols is a super-linear function of R_e or N_d and proportional to $e^{0.29\times R_e}$ or $N_d^{-1.5}$ indicating that the rate of Cf increase accelerates with cleaner background clouds with larger R_e. Quantitatively, the measured rate of Cf increase is at a rate of 1.2% per 1 cm^{-3} when the background N_d is at 9 cm^{-3}, which is very close to the simulated value of 1.4% per 1 cm^{-3} at the same background N_d in Possner et al.(*23*) using a large-eddy simulation model with detailed physics. At background N_d of 20 cm^{-3}, the rate decreases to 0.45% per 1 cm^{-3}. The tight exponential fit, $dCf/dN_d \propto e^{0.29\times R_e} \mid R_e > 14\mu m$, suggests that addition of aerosols can reverse the runaway depletion of cloud water and decrease of Cf by precipitation. Addition of aerosols in an aerosol-limited regime can strongly increase Cf, which qualitatively supports observations and modeling results of ship-emitted aerosols reversing low Cf scenes to nearly overcast ones (*11*, *12*, *22*, *23*). Our analyses show that the effects of aerosol-cloud-precipitation interactions on Cf are nonlinear and depend on background conditions(*29*, *30*). This measurement-based relationship provides valuable quantitative constraints on the Cf adjustments to aerosols under different background conditions.

The Cf adjustment also has clear dependence on the background Cf. On average, dCf/dN_d is negatively correlated with the background Cf. The sensitivity is at zero when background Cf is around 1 and peaks at about 3% per 1 cm^{-3} when the background Cf is about 0.2. Cf of 0.2 is notably lower than the mean Cf for open cellular clouds, at around 0.5 (*31*), and close to that of marine low clouds with heavy drizzle (*32*). The combination of low Cf and heavy drizzle points to an aerosol-limited cloud regime primed for high dCf/dN_d , which agrees with the relationship between dCf/dN_d and R_e and observations of ship-tracks appearing overcast within a low Cf and precipitating environment(*12*, *18*, *20*) (e.g., Figure 1).

The average LWP adjustment, $\overline{dLWP}$, is 5.83 gm^{-2} with a large standard deviation of 31 gm^{-2}. The fairly small $\overline{dLWP}$ results from substantial dLWP in both positive and negative directions in individual ship-track samples, reaffirming results from previous studies(*10*, *19–21*, *33*). 48% of the ship-track samples have negative dLWP even though $\overline{dLWP}$ is close to zero and positive. The relative sensitivity of LWP to N_d, $dlnLWP/dlnN_d$, is found to be a function of the background N_d (or R_e) and above cloud relative humidity(*10*, *24*). $dlnLWP/dlnN_d$ starts to be positive when above cloud relative humidity is greater than 85%, and N_d is less than 45 cm^{-3} (Figure 5). The dependence of LWP adjustment on above cloud relative humidity supports the idea that the balance between the effects of entrainment drying and moistening by precipitation suppression(*5*, *10*) partially determines the LWP adjustment. Its N_d dependence may reflect the aerosol effect on precipitation. The 45 cm^{-3} threshold suggests that once appreciable precipitation develops, aerosols tend to suppress the cloud water depletion by precipitation and increase LWP and Cf. When precipitation is not strong enough, the effect of drizzle suppression by aerosols on LWP can be counterbalanced by increased entrainment drying if the above cloud relative humidity is low(*34*). However, more factors may be at play

in the LWP adjustment than just the balance between precipitation suppression and entrainment drying such as cloud top height, boundary stability, and sea surface temperature (*10*).

Unlike LWP, the sensitivity of Cf to aerosols has weak dependence on the above cloud relative humidity (Figure 4). The mean dCf/dN_d is around 0.1% per cm^{-3} when averaged under most relative humidity values and its uncertainty range relative to the mean is considerably larger than that using background N_d or R_e as the explanatory variable. This suggests that above cloud relative humidity plays a minor role in determining Cf adjustment and supports the primary role of aerosol-cloud-precipitation interactions in driving Cf adjustment.

2.3 Forcing due to Cf and LWP adjustments

Our analysis shows that aerosols in ship-tracks make clouds brighter mainly through the Twomey effect with a minor contribution from the LWP adjustment because $\overline{dLWP}$ is only 5.83 g/m^2. But the range of LWP adjustments is wide and depends on background meteorology and cloud conditions, leading to a range of possible responses, from strong cancelation of the Twomey effect due to LWP reduction to strong enhancement by LWP increases. More importantly, ship-emitted aerosols also make the whole scene brighter by increasing Cf in addition to increasing existing clouds' brightness. The Cf adjustment is substantial (e.g. Figure 3) since an absolute increase of 3.5~5% in low Cf would be enough to counterbalance the positive forcing of CO_2 doubling (*35*, *36*), which suggests the Cf adjustment at local regions can be substantial. The Cf adjustment also depends sensitively on the background R_e or N_d, and Cf.

We quantify the relative contribution of the LWP and Cf adjustments to the total aerosol indirect forcing to that of the Twomey effect over global ocean. We apply the dependence of the dCf/dN_d and $dlnLWP/dlnN_d$ on the background N_d as measured in ship-tracks to global observations. The N_d change is produced by global chemical transport model simulations(*10*). We also consider the effects of cloud albedo, low cloud fraction, cloud overlap between high and low clouds, Cf change, and solar flux (see Method section for details). Our calculations show that the LWP adjustment effect is only adding 1% of radiative cooling to the Twomey effect when averaged over global oceans. The estimated forcing from the Twomey effect is -0.75 Wm^{-2} which is close to the consensus (*3)*. The forcing from the LWP adjustment represents an additional contribution of 1% on top of the Twomey effect, and is estimated to be -0.0083 ± 0.012 Wm^{-2} (Figure 6 & Table S1).

The effect of Cf adjustment, however, contributes an additional 52% cooling relative to the Twomey effect. The estimated radiative forcing from the Cf adjustment is -0.39 ± 0.01 Wm^{-2}. Our estimate would suggest the total aerosol indirect forcing to be -1.1 ± 0.8 Wm^{-2} given the current best estimate of the Twomey effect is -0.7 ± 0.5 Wm^{-2} (*3*, *7*). The absolute magnitudes of the forcing due to the two adjustments are subject to retrieval uncertainties in cloud variables and the estimated ΔN_d as discussed in detail in our Method section. Their relative contributions to the Twomey effect however are less sensitive to such uncertainties (see Method and (*10*).

3. **Discussion**

Our analysis of ship-tracks finds negligible global impact from the LWP adjustment, which supports the idea that the LWP adjustment is often overestimated, i.e., leading to excessively cooling effect, in current global climate models (GCMs)(*10*). However, it is quantitatively different from the strong warming effect reported in Toll et al.(*10*) that uses similar approach. The discrepancy can be explained by the different data filters applied on their ship-track samples. We can reproduce their $dlnLWP/dlnN_d$ dependence on R_e if we apply the same filters, i.e., only keeping samples whose ΔRe $> 2\mu$m and $\Delta N_d/N_d > 1$. But such filters remove 72% of the samples and result in a notable shift of sampled background cloud properties toward those with higher R_e and LWP (See Method and Figure S4), which drives the LWP adjustment to be more negative (Figure S5). Indeed, ΔRe and $\Delta N_d/N_d$ in ship-tracks depend on the background cloud conditions(*37*) and can have a wide range, with ΔRe peaking between 0 and 1μm(*20*, *38*). Taken to the extreme, ship-emitted aerosols can affect clouds and radiation budget without detectable ship-tracks(*23*, *39*). We believe that a less restrictive filter helps to obtain a more complete sampling of cloud conditions. Recent analysis indicates that LWP adjustment may produce strongly negative forcing in the so-called invisible ship-tracks(*40*).

The Cf adjustment is nonlinear and a function of multiple variables. We illustrate the sensitivity of the forcing from Cf adjustment to the choice of explanatory variables. Instead of a single explanatory variable, N_d, we calculate the dependence of the Cf adjustment as a function of two independent variables. The radiative forcing due to the Cf adjustment can be 212% of the Twomey effect, or -1.58 Wm^{-2}, if we use N_d and background SST as explanatory variables (see Figure S6 and Table S2). The estimates from using different combination of explanatory variables are summarized in Table S2 and they range from 51% to 396% of the Twomey effect with a mean of 180% and standard error of 53%. Since the multivariate approach should capture the nonlinearity more completely, our calculations suggest the true effect of Cf adjustment may be underestimated using a single explanatory variable, which provides a lower bound (Table S2).

The non-linear dependence of dCf/dN_d on N_d implies the effect of Cf adjustment is time-varying driven by the changing background N_d due to time-varying anthropogenic emissions. The Cf adjustment was the strongest when N_d was the lowest at preindustrial conditions(*29*, *41*). It would be stronger than its present value in regions downwind of major anthropogenic pollution sources like Northern Pacific and Atlantic Oceans where N_d has substantially increased by human activity. As a consequence, the preindustrial level of N_d can meaningfully affect both the time evolution and absolute magnitude of radiative forcing due to the Cf adjustment. It is therefore important to accurately estimate the preindustrial N_d because uncertainties in preindustrial N_d can translate into large uncertainties in Cf adjustment induced forcing due to large dCf/dN_d at low N_d, similar to the sensitivity of the Twomey effect to preindustrial N_d(*42*). For example, the forcing due to the Cf adjustment can increase by 10% if we uniformly decrease the background N_d by just 5 cm^{-3}. Finally, when estimating ΔN_d between preindustrial and present day, it is important to consider the effects of aerosol speciation on N_d (*43*).

A few issues remain unaddressed in our study. We do not explicitly consider the time dependence of Cf and LWP adjustments to aerosols(*24*, *44*, *45*) because our analyses are based on instantaneous data although part of the time-dependent adjustments are implicitly included because our dataset includes ship-tracks of various ages (*24*). We follow previous studies (*7*, *10*, *18*) and extrapolate results from ship-tracks to global ocean, which introduces uncertainty in our estimate of forcing. For example, LWP adjustment may introduce stronger

cooling inside the trade cumulus regime than inside the stratocumulus regime that is the dominant regime sampled here (*40*). Extrapolating Cf effect derived mainly from the stratocumulus regime to the trade cumulus regime may introduce uncertainty since case studies using large-eddy simulations and observational analyses suggest Cf can either decrease or increase in this regime (*6*, *15*, *30*). The potential choices of explanatory variables can also be expanded to include the underlying cloud morphology type and other cloud controlling factors. Several assumptions and approximations are also made in our calculations (see SOM). Our results are based on detectable ship-tracks, and we assume that given the same background clouds, they would have the same sensitivity to added aerosols and that sensitivity can be captured by detected ship-tracks. There are situations where clouds that are affected by ship-emitted aerosols, but do not produce detectable ship-tracks. It could be due to a combination of weak aerosol perturbation, already heavily polluted background clouds, unfavorable cloud types (*25*,*40*), and/or unknown processes. Future studies are needed to comprehensively address these issues to further improve our understanding.

In summary, the magnitude of the radiative cooling effect of the Cf adjustment can be on par with the Twomey effect(*16*, *30*, *46*). Our results, based on an unprecedented number of ship-track samples, suggest that it can range between 51% and 396% of the Twomey effect with a mean of 180%, which is in agreement with previous estimates with a range between 130% and 200% (*7*) using correlational analyses. GCMs also simulate Cf increase, primarily due to aerosols suppressing precipitation and increasing Cf (*41*). Process-level large-eddy simulations show notable Cf increase under clean conditions for stratocumulus clouds(*22*, *23*) while others show a slight decrease under different conditions, e.g. in the trade cumulus regime(*6*). Our analysis strongly supports a large cooling effect from the Cf adjustment under a variety of meteorological and cloud conditions that consistently show Cf increase with aerosols. The strong effect from Cf adjustment also points to clean and low Cf clouds as the most effective targets for climate intervention studies(*47*, *48*). The observation-based relationships between the Cf sensitivity to aerosols and background N_d and R_e provides a quantitative constraint and benchmark to improve aerosol-cloud parameterizations in GCMs, which may help to reduce the uncertainty in aerosol indirect forcing and increase the confidence in climate projections of the future.

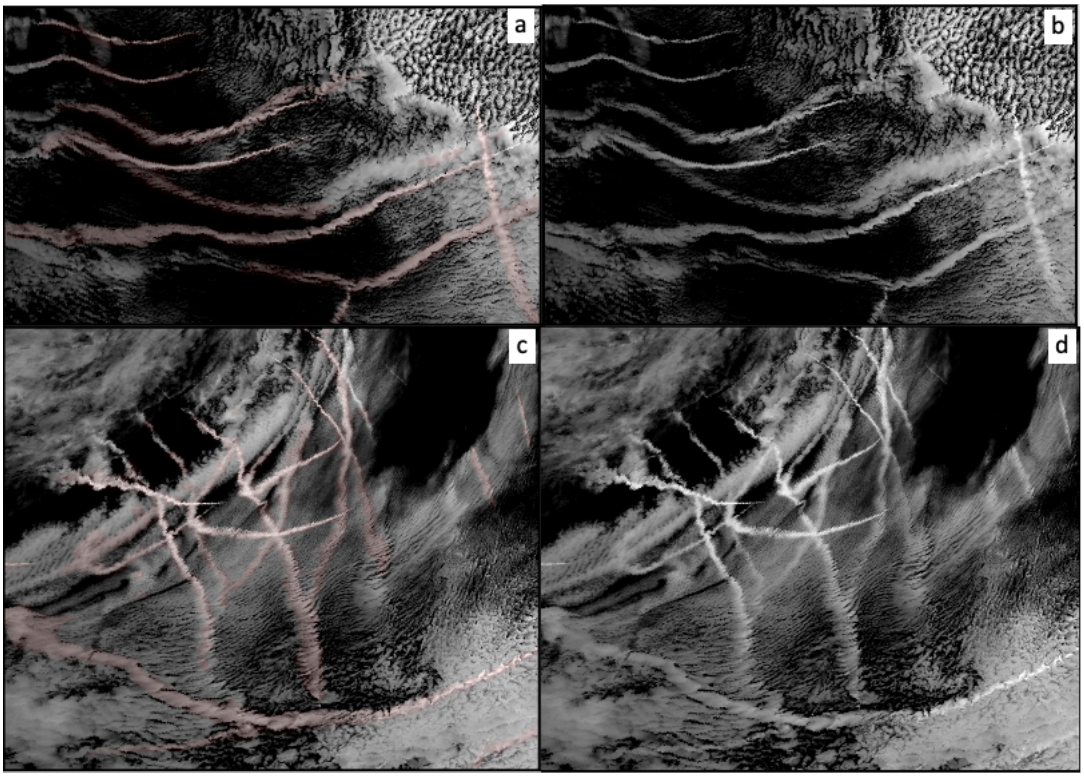

Figure 1 example images of ship-tracks and detected ship-track masks: MODIS Aqua images of 2.1 μm reflectance overlaid with detected ship-track mask in pink (a) and true color (b) at 21:25 UTC, June 29, 2005, and the same at 22:25 UTC, July 12, 2010 (c) and (d).

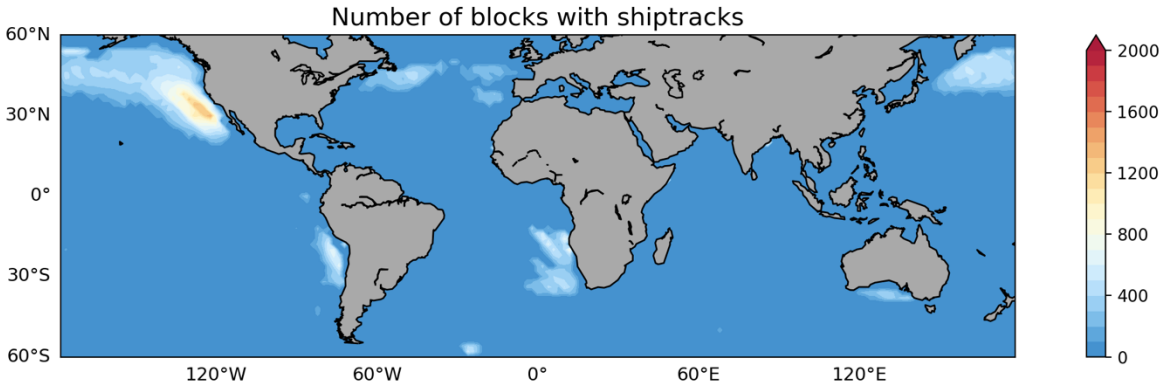

Figure 2 Frequency of ship-track containing blocks. The Northern Pacific has the most samples. Considerable number of samples also come from the southeast Pacific, the southeast Atlantic, the northern Atlantic, and to the south of Australia.

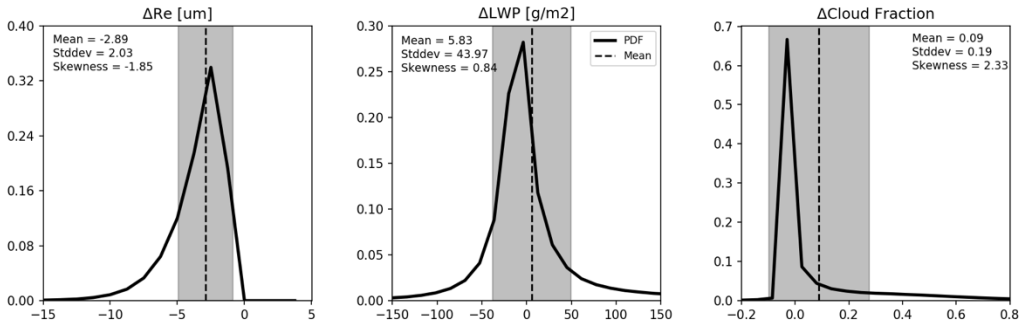

Figure 3 distributions of bulk cloud adjustments: PDFs of $\Delta R_e, \Delta LWP, and\ \Delta$Cf for individual 128pixelx128pixel MODIS blocks that contain ship-tracks (see Method). The mean values are indicated by the dashed vertical lines and the +/- one standard deviation range is in gray shading.

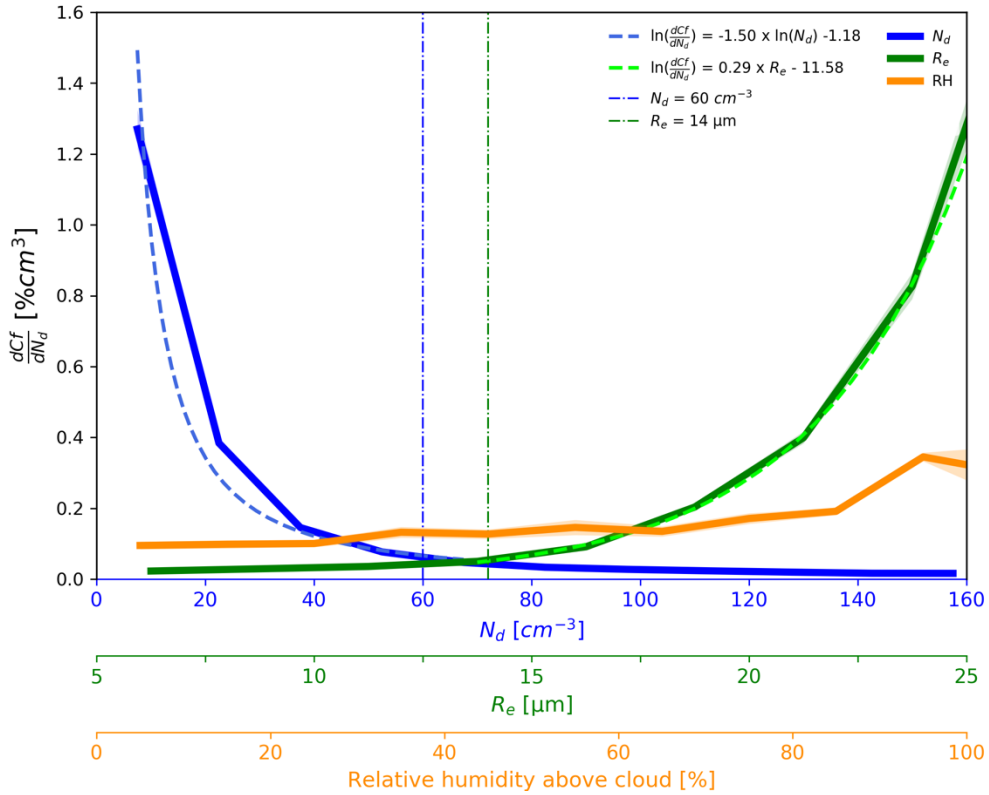

Figure 4 dependence of coverage adjustment on background conditions: dCf/dN_d for each bin of the background cloud N_d, R_e, and RH above the cloud, where Cf represents low cloud fraction. The blue and green dashed lines are functional fit to the data. The vertical dashed lines are for constant N_d and R_e at 60 cm^{-3} and 14 µm, respectively. Each solid, colored line has an x-axis with the same color and associated uncertainty range is plotted as shades around the solid line. The range represents the 5% to 95% range.

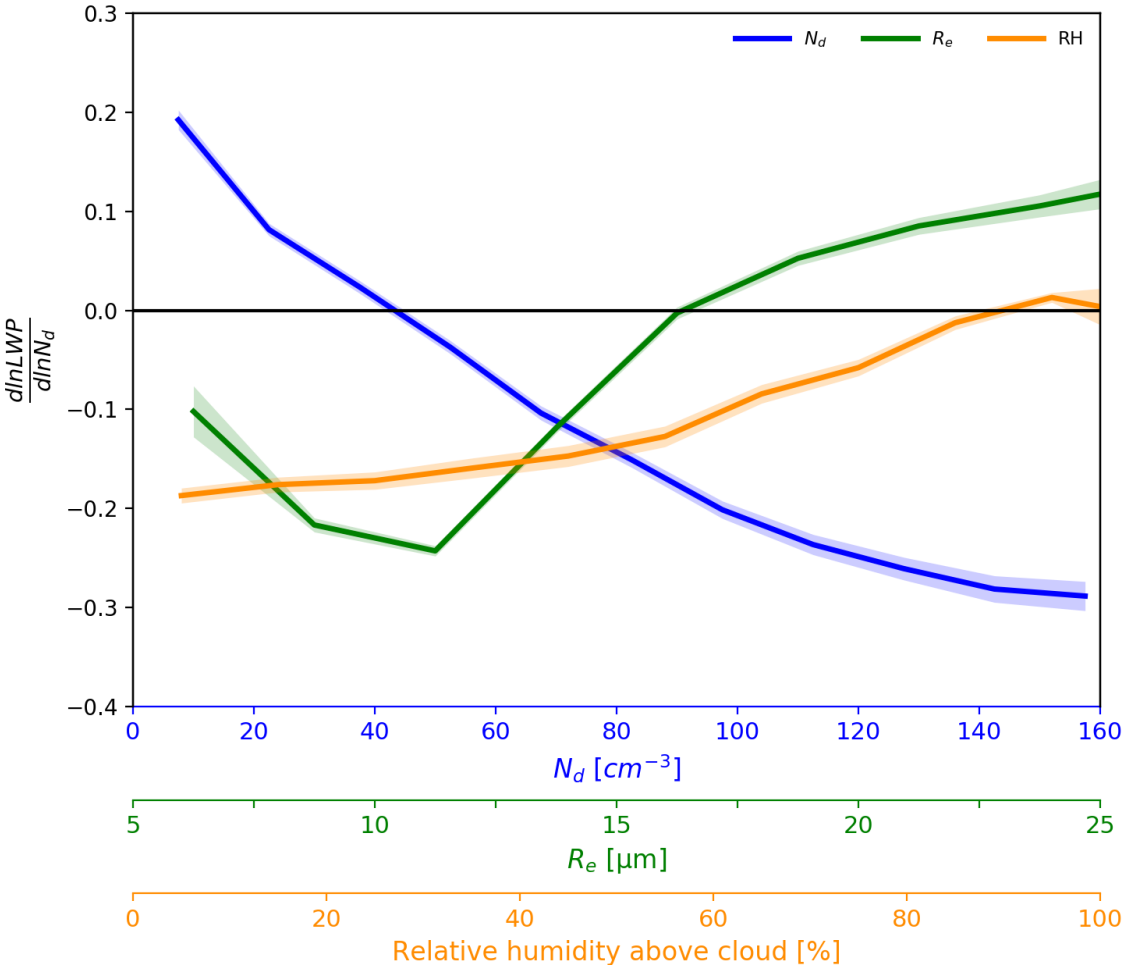

Figure 5 dependence of LWP adjustment on background conditions: the dependence of $dlnLWP/dlnN_d$ on above cloud top relative humidity, background R_e and N_d. Plot setup is similar to Figure 4.

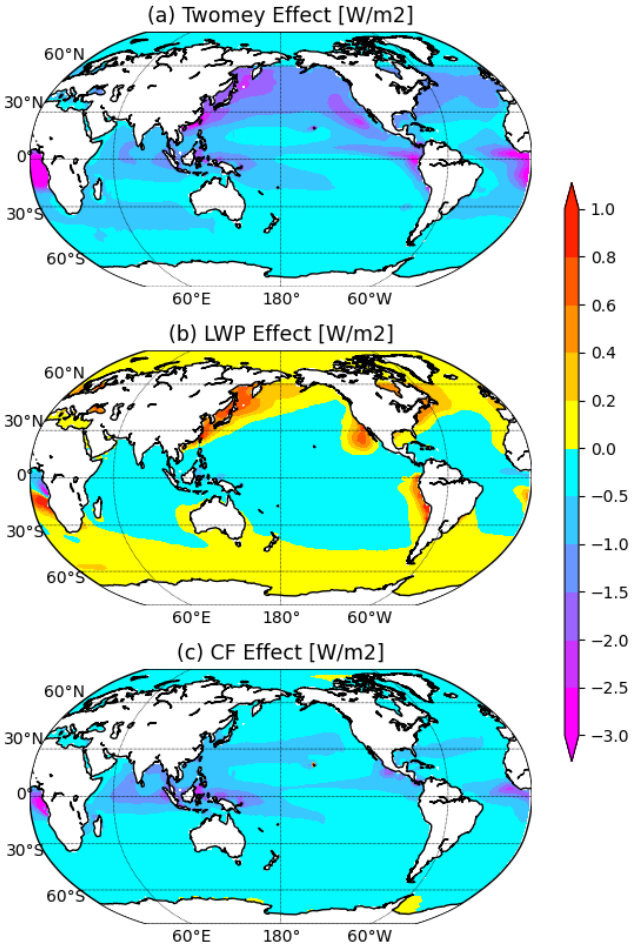

Figure 6 estimated forcings from different adjustments: The calculated aerosol indirect forcing contributions from the Twomey effect (a), the LWP adjustment (b), and the Cf adjustment (c).

4. Materials and Methods

Method:

As an overview, we derive LWP and Cf adjustments based on observations and analysis of ship-tracks. The key quantity to estimate is the ratio between forcings due to Cf and LWP adjustments and that of the Twomey effect with mostly observed variables. The ratio is fundamentally controlled by the sensitivity of Cf and LWP to N_d as shown by formulations discussed in detail in the following. While the absolute magnitudes of the Twomey effect, and the Cf and LWP adjustments are sensitive to assumptions made and estimated ΔN_d as well as retrieval uncertainties, the ratio is much less susceptible (*10)*. We have detailed discussions for the assumptions and potential sources of uncertainty in terms of the absolute magnitude in the following.

a. Analyzing cloud response in ship-tracks

For each detected ship-track, we automatically find background pixels in its surrounding. The width of these surrounding pixels is set to 20 pixels on both sides as shown in Figures S1 and S2. We do not include the one pixel just next to the edge of ship-track pixels to reduce the

uncertainty around the edge and minimize the impact of potential aerosol-induced circulation changes in some ship-track cases that can create a positive Cf change bias (*45*). We then break each granule into blocks of size 128pixel x 128pixel. Within each block, we calculate mean values of cloud variables such as droplet effective radius (R_e), cloud optical depth (COT), liquid water path (LWP) and cloud droplet number concentration (N_d) for the background and ship-track pixels. We consider the effect of cloud overlap when calculating Cf. We use the random overlap assumption: $Cf = (Cf_{total}-Cf_{high})/(1- Cf_{high})$, where Cf, Cf_{total} and Cf_{high} are low cloud fraction, total cloud fraction and high cloud fraction, respectively. The Cf calculation is carried out separately for pixels within ship-track and surrounding masks as illustrated by examples in Figure S2. The difference between cloud properties inside background and ship-track masks is taken as the cloud response to ship-emitted aerosols. It is worth noting that our method allows for Cf adjustment in both positive and negative directions.

Pixels for which the cloud phase determined by infrared observations was identified as ice or mixed-phase, and those with ice cloud retrievals are excluded. Only pixels with a single layer, according to MODIS cloud product multi-layer flag, and a low-level cloud (cloud top pressure > 650 hPa) were included. We also exclude the small ship-tracks that have less than 400 pixels because their size is too small to obtain accurate cloud fraction. The track segments were included in the analyses only when the Re difference between ship-track and background clouds was less than -0.5 μm and the relative changes of Nd, larger than 20%. We choose to filter the data this way because of small uncertainty range of Re retrievals and larger uncertainty in Nd. For Re, the relative uncertainty for liquid clouds range between 1.5% to around 10% (*17*) while it is 78% for Nd at the pixel level. Since each ship-track sample typically contains hundreds of pixels and ensemble mean can reduce the magnitude of uncertainty, we select the threshold to be 0.5μm and 20% for Re and Nd, respectively. This choice has minimal impact on the probability distributions of cloud properties when comparing the filtered clouds and all samples (e.g., Figure S4). Further decreasing of their thresholds makes the calculation of the adjustments, which are derivatives, prone to uncertainties in these two variables. In total, there are 295,036 such ship-track blocks that satisfy our conditions. If we follow the criteria $\Delta R_e > 2.0\mu m$ used in Toll et al.(*10*), the number of samples decreases to 164,626. If additional condition of $\Delta N_d/N_d > 1$ is applied(*10*), the number of samples decreases to 83,155, representing a more than 72% decrease. It is also worth noting that in this study, we do not use any proxy such as aerosol optical depth or aerosol index for N_d since we can confidently attribute the changes of N_d between ship-track and background clouds to aerosols.

We group blocks based on their background N_d, or other variable of choice, into to a number of bins. For each bin, we calculate mean cloud responses and their 95% uncertainty ranges based on samples that fall within this bin. The dependence of cloud responses to background cloud variables can thus be obtained using this approach. The approach can be extended to 2-D bins based on two explanatory variables, e.g., N_d and Cf, and we can obtain a 2-D cloud response function. Once the relationships and their uncertainty ranges are derived, we assume similar relationships apply in regions that do not have high numbers of ship-track samples, i.e. we assume the same physics apply(*10*).

b. Calculating Aerosol Indirect Forcing

Without considering aerosol effects on cloud fractions, cloud albedo sensitivity to aerosols can be taken as the sum of the Twomey effect and aerosol induced LWP adjustments(*10*):

$$S = \frac{dA_c}{dN_d} = \frac{A_c(1-A_c)}{3N_d} \times (1 + \frac{5}{2}\frac{dln\ LWP}{dln\ N_d}) \quad (1)$$

where S is the susceptibility of cloud albedo (A_c) to droplet number concentration N_d(*10*).

If we only consider the Twomey effect and LWP adjustment, we have

$$\Delta SW_{TOA} = -SW_{downwelling} \times Cf \times S \times \Delta N_d \quad (2)$$

Aerosol indirect forcing is therefore:

$$\Delta SW_{TOA} = -SW_{downwelling} \times Cf \times A_c \times (1 - A_c) \times (\frac{1}{3} + \frac{5}{6}\frac{dlnLWP}{dln\ N_d}) \times \Delta lnN_d \quad (3).$$

$SW_{downwelling}$ is shortwave flux at the clouds. It can be conservatively estimated using the CERES clear sky surface downwelling shortwave flux. Cf is low cloud fraction. We use the MODIS L3 product to derive it. A_c is the cloud albedo, it can be calculated from the CERES all-sky albedo (A_{allsky}), clear-sky albedo ($A_{clearsky}$) and total cloud fraction (Cf_{total}) using the equation $A_c = (A_{allsky} - (1 - Cf_{total}) \times A_{clearsky})/Cf_{total}$ (4)

The CERES and MODIS data we used are 2003-2020 monthly mean 1°x1° global data of the CERES EBAF-TOA(*49*) and the MYD08_M3(*50*) products, respectively. We calculated the 2003-2020 climatological-mean $SW_{downwelling}$, Cf, and A_c, and interpolated them to 2°x2° horizontal resolution.

From the analysis of cloud response in ship-tracks, we first calculated the relative differences in LWP (dlnLWP) and the relative differences in Nd ($dlnN_d$) between ship-track blocks and their control counterparts, and thereby derived their ratios $\frac{dlnLWP}{dln\ N_d}$ for all ship-track samples. We then sorted these $\frac{dlnLWP}{dln\ N_d}$ by their control cloud N_d, and calculated mean values of $\frac{dlnLWP}{dln\ N_d}$ for each control N_d bin. The dependence of $\frac{dlnLWP}{dln\ N_d}$ on N_d is used as our function to calculate the LWP adjustment. For global 2°x2° grids, we first calculated 2003-2020 climatological-mean N_d from the MYD08_M3 data. Based on the 1-D dependence of $\frac{dlnLWP}{dln\ N_d}$ on N_d, we derive the global gridded LWP adjustment sensitivity, $\frac{dlnLWP}{dln\ N_d}$. ΔlnN_d and ΔN_d is calculated in the same way as Toll et al.(*10*) It is based on model simulated AOD difference between preindustrial and present and empirical relationship between AOD and N_d. To make our results and those from Toll et al. comparable we adopt the same method. For details, please refer to their paper. With all these variables ready, we calculate the global gridded values of aerosol indirect forcing due to the LWP adjustment to N_d.

To consider the effect of Cf adjustment due to aerosols, we consider the sensitivity of scene albedo (A) to N_d. $A = A_{ac}\,Cf_{total} + A_s(1 - Cf_{total})$ (*51*). We have:

$$S^* = \frac{dA}{dN_d} = \frac{d(A_{ac}\,Cf_{total} + A_s(1-Cf_{total}))}{dN_d} \approx Cf \times S + \left(1 - Cf_{high}\right) \times \frac{dCf}{dN_d} \times (A_{ac} - A_s) \quad (5)$$

where A is the scene albedo, i.e., including both cloudy, A_{ac}, and clear, A_s, parts; Cf_{total} and Cf are all cloud and low cloud fraction obtained from the MYD08_M3 data; A_s is the surface albedo, derived from the CERES EBAF-TOA data(*49*); $1 - Cf_{high}$ is used to take into account of effect of overlap on Cf adjustment. We assume minimum aerosol effects on high clouds. $\frac{dCf}{dN_d}$ is calculated using our ship-track samples, similar to the LWP adjustment. We account for the cloud overlap between high and low clouds when calculating Cf for both background and ship-track clouds to reflect its true values. Here we use the random overlap assumption, but tests

with other overalp assumptions show minimum impact. We first calculate $\frac{dCf}{dN_d}$ for each ship-track sample and sort them by their corresponding control cloud N_d. We then average values of $\frac{dCf}{dN_d}$ for each control N_d bin and obtain the 1-D dependence of $\frac{dCf}{dN_d}$ on N_d. On lat-lon grid, $\frac{dCf}{dN_d}$ is obtained based on its N_d according to the $\frac{dCf}{dN_d}$ vs N_d relationship, similar to the LWP adjustment (*10)*.

In addition, we calculate $\frac{dCf}{dN_d}$ and average them as a function of a pair of explanatory variables such as N_d - Cf , N_d - $EIS, and\ N_d - SST$. We then obtain the two-dimensional dependence of $\frac{dCf}{dN_d}$ on N_d and Cf, or other paired variables. Using this 2-D dependence of $\frac{dCf}{dN_d}$, we derive global gridded $\frac{dCf}{dN_d}$, and calculate S^* and changes of TOA SW flux due to cloud coverage effect using the equation:

$$\Delta SW_{TOA} = -SW_{downwelling} \times S^* \times \Delta N_d \qquad (6).$$

To study the influences of meteorological conditions on the Cf adjustments to aerosols, we collocate the MERRA2 2-dimensional hourly (inst1_2d_asm_Nx) data and 3-dimensional 3-hourly (inst3_3d_asm_Np) reanalysis data(*52*) with our ship-track and control clouds. We calculate mean values of the collocated MERRA2 relative humidity (RH), sea surface temperature (SST) and estimated inversion strength (EIS) for every ship-track block and background clouds. The Cf adjustments of individual ship-track sample are averaged based on the explanatory variable or pair of explanatory variables such as control cloud N_d, N_d and SST, and N_d and EIS. We thus obtain the 2-D dependence of $\frac{dCf}{dN_d}$ on N_d and Cf, N_d and SST, and N_d and EIS, respectively. Using these 2-D $\frac{dCf}{dN_d}$ dependences as the lookup table, we derived global gridded $\frac{dCf}{dN_d}$, and then calculated S^* and cloud coverage effects on the TOA SW flux. We also tried to derive 3-D dependence of $\frac{dCf}{dN_d}$ on N_d, EIS, and RH, and N_d, Cf, and RH. Similarly, we calculate the $\frac{dlnLWP}{dln\ N_d}$ and its dependence on background RH, EIS, and SST using the MERRA-2 data.

We propagate the uncertainties of our estimates of $\frac{dCf}{dN_d}$ and $\frac{dlnLWP}{dln\ N_d}$ and their dependence on N_d to uncertainty in forcing estimates. For each N_d, we find the 95% or 99% confidence intervals for the mean values of $\frac{dCf}{dN_d}$ and $\frac{dlnLWP}{dln\ N_d}$. We then apply the upper and lower limits of the Cf and LWP sensitivity to each grid point and obtain the upper and lower bound for indirect forcing due to Cf and LWP adjustments. The results are presented in Table S1. The forcing due to the LWP adjustment has a relatively larger range than that of the Cf adjustment.

The total forcing calculated using different sets of explanatory variables including N_d and Cf, N_d and SST, and N_d and EIS is presented in Table S2. For reference, we also include the number when using only N_d. Adding above cloud relative humidity does not appreciably change the forcing, which agrees with our finding that the Cf adjustment is not sensitive to above cloud RH. The largest forcing is obtained with the N_d and Cf combination and it represents more than 396% of the Twomey effect. The ratios are 212% and 75% when using N_d

and SST, and N_d and EIS, respectively. We also test with using three explanatory variables. The ratios are 384% and 97% when N_d, Cf, and RH, and N_d, EIS, and RH are used, respectively. In all, the range spans between 51% to 396% and the mean of ratios is 180% with a standard error of 53%.

We note a few assumptions and approximations adopted in our method of estimating the absolute aerosol indirect forcing detailed above. It is worth noting again that the ratio between effects of LWP and Cf adjustments and the Twomey effect is less susceptible to such assumptions. For example, the change in N_d can be substantial such that the condition $dlnN_d \ll 1$ is not satisfied and an integration is required to more accurately calculate the forcing . Similarly, an integration should be applied to the LWP and Cf adjustment calculations. We adopted the approximation because we do not know the exact functional form of the LWP and Cf adjustments and we want to compare the relative importance of the Twomey and the adjustment effects[7, 10]; We used $SW_{downwelling}$ at the surface from CERES in equation (2) instead of $SW_{downwelling}$ at the cloud top, which underestimates the total forcing since $SW_{downwelling}$ at the cloud top is larger. At the same time, we do not account for the transmittance from cloud top to the top of the atmosphere, which overestimates the forcing. This assumption is made because of the lack of observations for these quantities; finally, the LWP and Cf adjustments can be sensitive to more variables that are considered here. We adopted such approximations and assumptions due to the limit of observables (e.g., the $SW_{downwelling}$) and amount of available data (e.g., sensitivity of $\frac{dCf}{dN_d}$ and $\frac{dlnLWP}{dln\,N_d}$ to multiple variables). Also, we assume the derived $\frac{dCf}{dN_d}$ and $\frac{dlnLWP}{dln\,N_d}$ and their dependence on background variables apply to regions that have less ship-track samples. Here our goal is to provide a first estimate of the ratio based on best available observations and practices in the literature while being aware of such assumptions and approximations(*7*, *10*). Also, potential semi-direct effects due to absorbing aerosols from ship-emissions are not explicitly addressed in this study since we do not have enough observational information to separate it out.

Acknowledgments

General: We thank Dr. Patrick Chuang and the editor, Dr. Chiang, for their helpful comments and suggestions that improved the paper's quality.

Author Contributions: T. Yuan conceived the idea, designed the experiments and wrote the draft. All authors contributed to the writing of the manuscript and discussion of the results. H. Song conducted the data processing.

Funding: Funding is supported by the National Aeronautics and Space Administration [grant numbers: 80NSSC18M0084 and NNH20ZDA001N-TASNPP].

Conflicts of Interest

The authors declare that there is no conflict of interest regarding the publication of this article.

Data Availability

The MODIS cloud product, CERES flux and albedo product, and the MERRA2 data used in this study are available from the Atmosphere Archive and Distribution System (LAADS) Distributed Active Archive Center (DAAC), https://ladsweb.nascom.nasa.gov/, the https://ceres.larc.nasa.gov/data/, and the Global Modeling and Assimilation Office, https://gmao.gsfc.nasa.gov/reanalysis/MERRA-2/data_access/. The ship-track blocks data is available at https://doi.org/10.7910/DVN/JII4DN. All data needed to evaluate the conclusions in the paper are present in the paper and/or the Supplementary Materials.

References

1. S. Twomey, Influence of pollution on shortwave albedo of clouds. *Journal Of The Atmospheric Sciences*. **34**, 1149–1152 (1977).

2. B. Albrecht, Aerosols, Cloud Microphysics, and Fractional Cloudiness. *Science*. **245**, 1227 (1989).

3. P. Forster, T. Storelvmo, K. Armour, W. Collins, J.-L. Dufresne, D. Frame, D. J. Lunt, T. Mauritsen, M. D. Palmer, M. Watanabe, M. Wild, H. Zhang, "The Earth's Energy Budget, Climate Feedbacks, and Climate Sensitivity" in *Climate Change 2021: The Physical Science Basis. Contribution of Working Group I to the Sixth Assessment Report of the Intergovernmental Panel on Climate Change* (Cambridge University Press, 2021).

4. D. Victor, D. Zhou, E. H. M. Ahmed, P. K. Dadhich, J. Olivier, H.-H. Rogner, K. Sheikho, M. Yamaguchi, "Introductory chapter" in *AR5 Climate Change 2014: Mitigation of Climate Change from Working Group III* (Cambridge University Press, 2014).

5. A. S. Ackerman, M. P. Kirkpatrick, D. E. Stevens, O. B. Toon, The impact of humidity above stratiform clouds on indirect aerosol climate forcing. *Nature*. **432**, 1014–1017 (2004).

6. B. Stevens, G. Feingold, Untangling aerosol effects on clouds and precipitation in a buffered system. *Nature*. **461**, 607–613 (2009).

7. N. Bellouin, J. Quaas, E. Gryspeerdt, S. Kinne, P. Stier, D. Watson-Parris, O. Boucher, K. S. Carslaw, M. Christensen, A.-L. Daniau, J.-L. Dufresne, G. Feingold, S. Fiedler, P. Forster, A. Gettelman, J. M. Haywood, U. Lohmann, F. Malavelle, T. Mauritsen, D. T. McCoy, G. Myhre, J. Mülmenstädt, D. Neubauer, A. Possner, M. Rugenstein, Y. Sato, M. Schulz, S. E. Schwartz, O. Sourdeval, T. Storelvmo, V. Toll, D. Winker, B. Stevens, *Reviews of Geophysics*, 2020, doi:10.1029/2019RG000660.

8. Y.-C. Chen, M. W. Christensen, G. L. Stephens, J. H. Seinfeld, Satellite-based estimate of global aerosol–cloud radiative forcing by marine warm clouds. *Nature Geosci*. **7**, 643–646 (2014).

9. M. D. Lebsock, G. L. Stephens, C. Kummerow, Multisensor satellite observations of aerosol effects on warm clouds. *Journal of Geophysical Research: Atmospheres*. **113** (2008), doi:10.1029/2008JD009876.

10. V. Toll, M. Christensen, J. Quaas, N. Bellouin, Weak average liquid-cloud-water response to anthropogenic aerosols. *Nature*. **572**, 51–55 (2019).

11. D. Rosenfeld, Y. J. Kaufman, I. Koren, Switching cloud cover and dynamical regimes from open to closed Benard cells in response to the suppression of precipitation by aerosols. *Atmospheric Chemistry and Physics*. **6**, 2503–2511 (2006).

12. T. Goren, D. Rosenfeld, Satellite observations of ship emission induced transitions from broken to closed cell marine stratocumulus over large areas. *Journal of Geophysical Research: Atmospheres*. **117** (2012), doi:10.1029/2012JD017981.

13. Y. Wang, X. Zheng, X. Dong, B. Xi, P. Wu, T. Logan, Y. L. Yung, Impacts of long-range transport of aerosols on marine-boundary-layer clouds in the eastern North Atlantic. *Atmospheric Chemistry and Physics*. **20**, 14741–14755 (2020).

14. M. W. Christensen, W. K. Jones, P. Stier, Aerosols enhance cloud lifetime and brightness along the stratus-to-cumulus transition. *PNAS*. **117**, 17591–17598 (2020).

15. D. Rosenfeld, Y. Zhu, M. Wang, Y. Zheng, T. Goren, S. Yu, Aerosol-driven droplet concentrations dominate coverage and water of oceanic low-level clouds. *Science* (2019), doi:10.1126/science.aav0566.

16. E. Gryspeerdt, J. Quaas, N. Bellouin, Constraining the aerosol influence on cloud fraction. *Journal of Geophysical Research: Atmospheres*. **121**, 3566–3583 (2016).

17. D. P. Grosvenor, O. Sourdeval, P. Zuidema, A. Ackerman, M. D. Alexandrov, R. Bennartz, R. Boers, B. Cairns, J. C. Chiu, M. Christensen, H. Deneke, M. Diamond, G. Feingold, A. Fridlind, A. Hünerbein, C. Knist, P. Kollias, A. Marshak, D. McCoy, D. Merk, D. Painemal, J. Rausch, D. Rosenfeld, H. Russchenberg, P. Seifert, K. Sinclair, P. Stier, B. van Diedenhoven, M. Wendisch, F. Werner, R. Wood, Z. Zhang, J. Quaas, Remote Sensing of Droplet Number Concentration in Warm Clouds: A Review of the Current State of Knowledge and Perspectives. *Reviews of Geophysics*. **56**, 409–453 (2018).

18. M. W. Christensen, A. Gettelman, J. Cermak, G. Dagan, M. Diamond, A. Douglas, G. Feingold, F. Glassmeier, T. Goren, D. P. Grosvenor, E. Gryspeerdt, R. Kahn, Z. Li, P.-L. Ma, F. Malavelle, I. L. McCoy, D. T. McCoy, G. McFarquhar, J. Mülmenstädt, S. Pal, A. Possner, A. Povey, J. Quaas, D. Rosenfeld, A. Schmidt, R. Schrödner, A. Sorooshian, P. Stier, V. Toll, D. Watson-Parris, R. Wood, M. Yang, T. Yuan, Opportunistic experiments to constrain aerosol effective radiative forcing. *Atmospheric Chemistry and Physics*. **22**, 641–674 (2022).

19. Y.-C. Chen, M. W. Christensen, L. Xue, A. Sorooshian, G. L. Stephens, R. M. Rasmussen, J. H. Seinfeld, Occurrence of lower cloud albedo in ship tracks. *Atmospheric Chemistry and Physics*. **12**, 8223–8235 (2012).

20. M. W. Christensen, G. L. Stephens, Microphysical and macrophysical responses of marine stratocumulus polluted by underlying ships: Evidence of cloud deepening. *Journal of Geophysical Research*. **116**, D03201 (2011).

21. S. Hu, Y. Zhu, D. Rosenfeld, F. Mao, X. Lu, Z. Pan, L. Zang, W. Gong, The Dependence of Ship-Polluted Marine Cloud Properties and Radiative Forcing on Background Drop Concentrations. *Journal of Geophysical Research: Atmospheres*. **126** (2021), doi:10.1029/2020JD033852.

22. H. Wang, P. J. Rasch, G. Feingold, Manipulating marine stratocumulus cloud amount and albedo: a process-modelling study of aerosol-cloud-precipitation interactions in response to injection of cloud condensation nuclei. *Atmospheric Chemistry And Physics*. **11**, 4237–4249 (2011).

23. A. Possner, H. Wang, R. Wood, K. Caldeira, T. P. Ackerman, The efficacy of aerosol–cloud radiative perturbations from near-surface emissions in deep open-cell stratocumuli. *Atmospheric Chemistry and Physics*. **18**, 17475–17488 (2018).

24. E. Gryspeerdt, T. Goren, T. W. P. Smith, "Observing the timescales of aerosol-cloud interactions in snapshot satellite images" (2020), , doi:10.5194/acp-2020-1030.

25. T. Yuan, H. Song, C. Wang, L. Oreopoulos, S. E. Platnick, S. von Hippel, K. G. Meyer, S. Light, E. Wilcox, Global Reduction in Ship-tracks from Sulfur Regulations for Shipping Fuel. *Science Advances*.(2022).

26. T. Yuan, C. Wang, H. Song, S. Platnick, K. Meyer, L. Oreopoulos, Automatically Finding Ship Tracks to Enable Large-Scale Analysis of Aerosol-Cloud Interactions. *Geophysical Research Letters*. **46**, 7726–7733 (2019).

27. R. Wood, C. S. Bretherton, On the relationship between stratiform low cloud cover and lower-tropospheric stability. *Journal Of Climate* (2006) (available at http://journals.ametsoc.org/doi/pdf/10.1175/JCLI3988.1).

28. D. Rosenfeld, H. Wang, P. J. Rasch, The roles of cloud drop effective radius and LWP in determining rain properties in marine stratocumulus. *Geophysical Research Letters*. **39** (2012), doi:10.1029/2012GL052028.

29. I. Koren, G. Dagan, O. Altaratz, From aerosol-limited to invigoration of warm convective clouds. *Science* (2014), doi:10.1126/science.1252595.

30. T. Yuan, L. A. Remer, H. Yu, Microphysical, macrophysical and radiative signatures of volcanic aerosols in trade wind cumulus observed by the A-Train. *Atmospheric Chemistry And Physics*. **11**, 7119–7132 (2011).

31. R. Wood, D. L. Hartmann, Spatial variability of liquid water path in marine low cloud: The importance of mesoscale cellular convection. *Journal Of Climate*. **19**, 1748–1764 (2006).

32. A. Muhlbauer, I. L. McCoy, R. Wood, Climatology of stratocumulus cloud morphologies: microphysical properties and radiative effects. *Atmospheric Chemistry And Physics*. **14**, 6695–6716 (2014).

33. F. F. Malavelle, J. M. Haywood, A. Jones, A. Gettelman, L. Clarisse, S. Bauduin, R. P. Allan, I. H. H. Karset, J. E. Kristjánsson, L. Oreopoulos, N. Cho, D. Lee, N. Bellouin, O. Boucher, D. P. Grosvenor, K. S. Carslaw, S. Dhomse, G. W. Mann, A. Schmidt, H. Coe, M. E. Hartley, M. Dalvi, A. A. Hill, B. T. Johnson, C. E. Johnson, J. R. Knight, F. M. O'Connor, D. G. Partridge, P. Stier, G. Myhre, S. Platnick, G. L. Stephens, H. Takahashi, T. Thordarson, Strong constraints on aerosol–cloud interactions from volcanic eruptions. *Nature*. **546**, 485–491 (2017).

34. C. R. Terai, M. S. Pritchard, P. Blossey, C. S. Bretherton, *Journal of Advances in Modeling Earth Systems*, 2020, doi:10.1029/2020MS002274.

35. A. Slingo, Sensitivity of the Earth's radiation budget to changes in low clouds. *Nature*. **343**, 49–51 (1990).

36. D. A. Randall, J. A. Coakley, C. W. Fairall, R. A. Kropfli, D. H. Lenschow, Outlook for Research on Subtropical Marine Stratiform Clouds. *Bulletin of the American Meteorological Society*. **65**, 1290–1301 (1984).

37. S. Platnick, P. A. Durkee, K. Nielsen, J. P. Taylor, S. C. Tsay, M. D. King, R. J. Ferek, P. V. Hobbs, J. W. Rottman, The Role of Background Cloud Microphysics in the Radiative Formation of Ship Tracks. *Journal Of The Atmospheric Sciences*. **57**, 2607–2624 (2000).

38. P. A. Durkee, K. J. Noone, R. J. Ferek, D. W. Johnson, J. P. Taylor, T. J. Garrett, P. V. Hobbs, J. G. Hudson, C. S. Bretherton, G. Innis, G. M. Frick, W. A. Hoppel, C. D. O'Dowd, L. M. Russell, R. Gasparovic, K. E. Nielsen, S. A. Tessmer, E. Öström, S. R. Osborne, R. C. Flagan, J. H. Seinfeld, H. Rand, The Impact of Ship-Produced Aerosols on the Microstructure and Albedo of Warm Marine Stratocumulus Clouds: A Test of MAST Hypotheses 1i and 1ii. *Journal of the Atmospheric Sciences*. **57**, 2554–2569 (2000).

39. M. S. Diamond, H. M. Director, R. Eastman, A. Possner, R. Wood, *AGU Advances*, 2020, doi:https://doi.org/10.1029/2019AV000111.

40. P. Manshausen, D. Watson-Parris, M. W. Christensen, J.-P. Jalkanen, P. Stier, Invisible ship tracks show large cloud sensitivity to aerosol. *Nature*. **610**, 101–106 (2022).

41. S. Ghan, M. Wang, S. Zhang, S. Ferrachat, A. Gettelman, J. Griesfeller, Z. Kipling, U. Lohmann, H. Morrison, D. Neubauer, D. G. Partridge, P. Stier, T. Takemura, H. Wang, K. Zhang, Challenges in constraining anthropogenic aerosol effects on cloud radiative forcing using present-day spatiotemporal variability. *Proc Natl Acad Sci U S A*. **113**, 5804–5811 (2016).

42. K. S. Carslaw, L. A. Lee, C. L. Reddington, K. J. Pringle, A. Rap, P. M. Forster, G. W. Mann, D. V. Spracklen, M. T. Woodhouse, L. A. Regayre, J. R. Pierce, Large contribution of natural aerosols to uncertainty in indirect forcing. *Nature*. **503**, 67–71 (2013).

43. P. V. Hobbs, T. J. Garrett, R. J. Ferek, S. R. Strader, D. A. Hegg, G. M. Frick, W. A. Hoppel, R. F. Gasparovic, L. M. Russell, D. W. Johnson, C. O'Dowd, P. A. Durkee, K. E. Nielsen, G. Innis, Emissions from Ships with respect to Their Effects on Clouds. *Journal of the Atmospheric Sciences*. **57**, 2570–2590 (2000).

44. F. Glassmeier, F. Hoffmann, J. S. Johnson, T. Yamaguchi, K. S. Carslaw, G. Feingold, Aerosol-cloud-climate cooling overestimated by ship-track data. *Science*. **371**, 485–489 (2021).

45. H. Wang, G. Feingold, Modeling Mesoscale Cellular Structures and Drizzle in Marine Stratocumulus. Part II: The Microphysics and Dynamics of the Boundary Region between Open and Closed Cells. *Journal Of The Atmospheric Sciences*. **66**, 3257–3275 (2009).

46. M. W. Christensen, D. Neubauer, C. A. Poulsen, G. E. Thomas, G. R. McGarragh, A. C. Povey, S. R. Proud, R. G. Grainger, Unveiling aerosol–cloud interactions – Part 1: Cloud

contamination in satellite products enhances the aerosol indirect forcing estimate. *Atmospheric Chemistry and Physics*. **17**, 13151–13164 (2017).

47. R. Wood, Assessing the potential efficacy of marine cloud brightening for cooling Earth using a simple heuristic model. *Atmospheric Chemistry and Physics Discussions*, 1–52 (2021).

48. Y. Chen, J. Haywood, Y. Wang, F. Malavelle, G. Jordan, D. Partridge, J. Fieldsend, J. De Leeuw, A. Schmidt, N. Cho, L. Oreopoulos, S. Platnick, D. Grosvenor, P. Field, U. Lohmann, Machine learning reveals climate forcing from aerosols is dominated by increased cloud cover. *Nat. Geosci.* **15**, 609–614 (2022).

49. N. G. Loeb, D. R. Doelling, H. Wang, W. Su, C. Nguyen, J. G. Corbett, L. Liang, C. Mitrescu, F. G. Rose, S. Kato, Clouds and the Earth's Radiant Energy System (CERES) Energy Balanced and Filled (EBAF) Top-of-Atmosphere (TOA) Edition-4.0 Data Product. *Journal of Climate*. **31**, 895–918 (2018).

50. S. Platnick, K. G. Meyer, M. D. King, G. Wind, N. Amarasinghe, B. Marchant, G. T. Arnold, Z. Zhang, P. A. Hubanks, R. E. Holz, P. Yang, W. L. Ridgway, J. Riedi, The MODIS Cloud Optical and Microphysical Products: Collection 6 Updates and Examples From Terra and Aqua. *IEEE Transactions on Geoscience and Remote Sensing*. **55**, 502–525 (2017).

51. M. Webb, C. Senior, S. Bony, J.-J. Morcrette, Combining ERBE and ISCCP data to assess clouds in the Hadley Centre, ECMWF and LMD atmospheric climate models. *Climate Dynamics*. **17**, 905–922 (2001).

52. R. Gelaro, W. McCarty, M. J. Suárez, R. Todling, A. Molod, L. Takacs, C. A. Randles, A. Darmenov, M. G. Bosilovich, R. Reichle, K. Wargan, L. Coy, R. Cullather, C. Draper, S. Akella, V. Buchard, A. Conaty, A. M. da Silva, W. Gu, G.-K. Kim, R. Koster, R. Lucchesi, D. Merkova, J. E. Nielsen, G. Partyka, S. Pawson, W. Putman, M. Rienecker, S. D. Schubert, M. Sienkiewicz, B. Zhao, The Modern-Era Retrospective Analysis for Research and Applications, Version 2 (MERRA-2). *J. Climate*. **30**, 5419–5454 (2017).

Supplementary Materials

Table S1: [60º S ~ 60º N] Global Ocean Mean Forcing (W/m^2)

Method	LWP Effect	Cf Effect
mean	-8.3×10^{-3}	-0.38
95% interval	$[-2.1\times10^{-2}, 4\times10^{-3}]$	[-0.4, -0.37]
99% interval	$[-2.5\times10^{-2}, 8.4\times10^{-3}]$	[-0.4, -0.36]

Table S2: Forcing Using Different Explanatory Variables (W/m^2)

Explanatory variable(s)	Cf Effect/Twomey
N_d only	52%
N_d and Cf	396%
N_d and RH	51%
N_d and SST	212%
N_d and EIS	75%
N_d, Cf, and RH	384%
N_d, EIS, and RH	97%

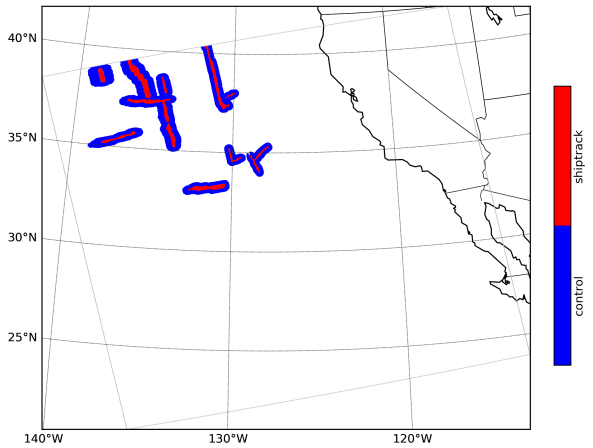

Figure S1: Detected ship-track pixels and their background pixels for an Aqua granule taken at 21:40 UTC on July 17, 2018. The width of the background (blue color in the figure) is 20 pixels.

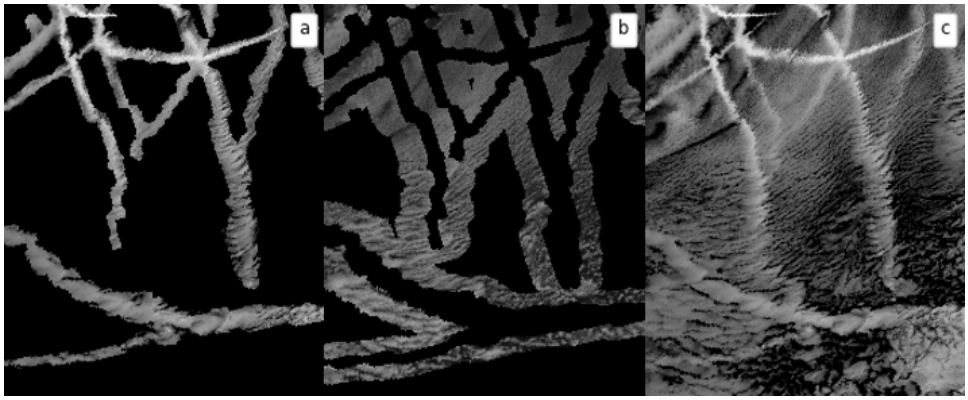

Figure S2: Examples of how to calculate cloud responses using ship-track and surrounding pixel masks. Pixels within ship-track and surrounding masks (a and b, respectively) and the full cloud scene (c). We calculate Cf for data within ship-track and surrounding masks. A pixel does not have to be cloudy to be included in ship-track or surrounding masks.

60

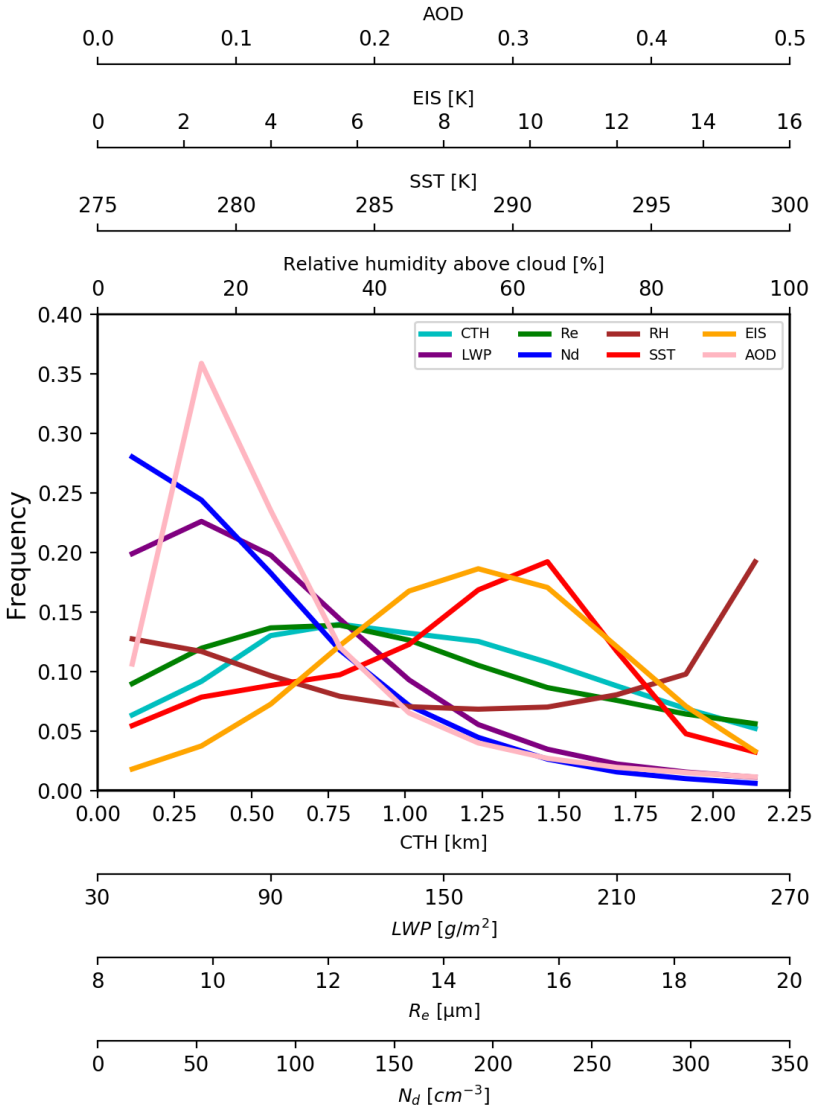

61

Figure S3 The frequency distribution of the background cloud properties: cloud top height (CTH), LWP, effective radius (Re), and N_d and background meteorological factors: sea surface temperature (SST), estimated inversion strength (EIS), RH and AOD, for all ship-tracks samples.

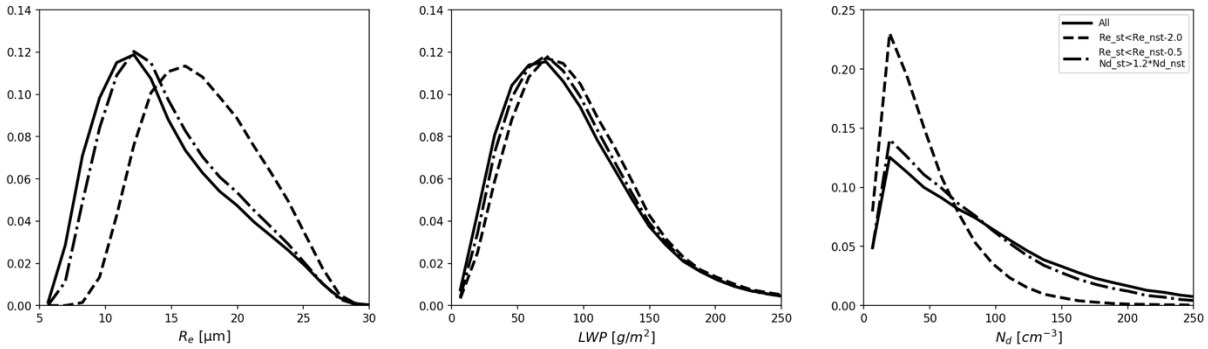

Figure S4 the impact of data filtering on sample distribution: PDFs of CER, LWP, and N_d for all samples, filter used by Toll et al.(*10*), and filter used here. Substantial shifts can be noticed for each cloud variable using the dCER > 2μm filter, which results in different $\frac{dlnLWP}{dln\,N_d}$ functions as shown in Figure S5.

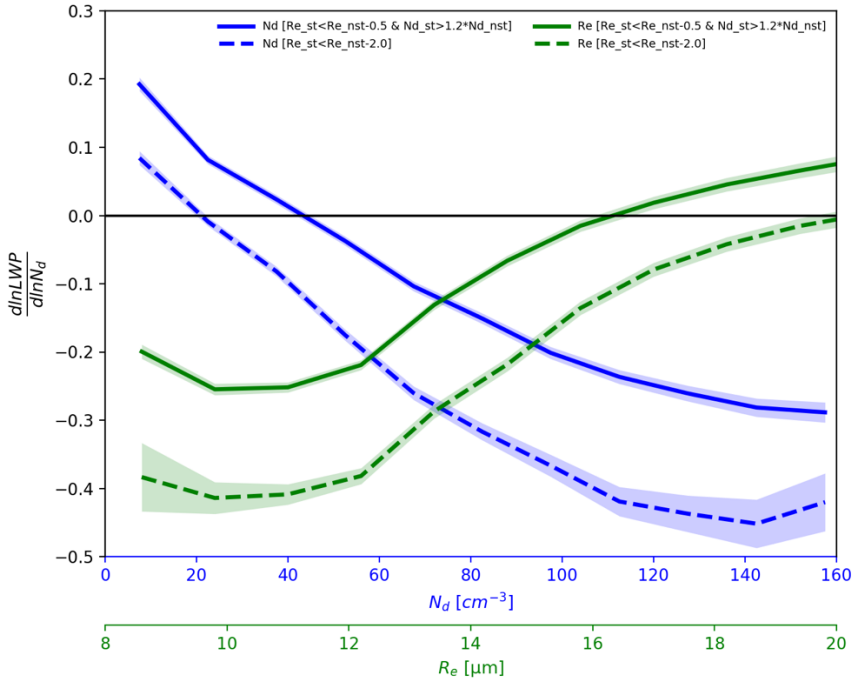

Figure S5 LWP adjustment using different data filters: the dependence of on dlnLWP/dlnNd on background N_d and Re, under different filters. Similar to Figures 4&5, the shades represent 5-95% range. With more restrictive filtering, the uncertainty range becomes slightly larger.

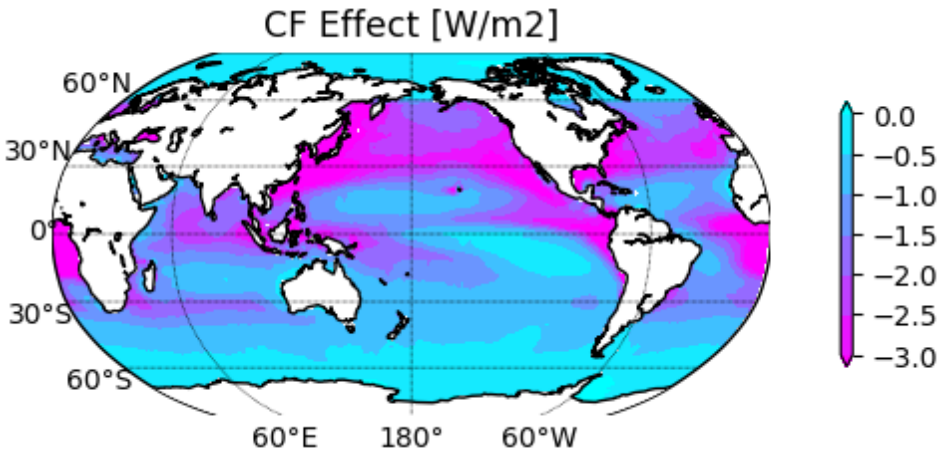

Figure S6 Cf adjustment forcing using N_d-Cf as explanatory variables: The calculated aerosol indirect forcing contributions from the Cf adjustment, using background N_d and Cf as explanatory variables.

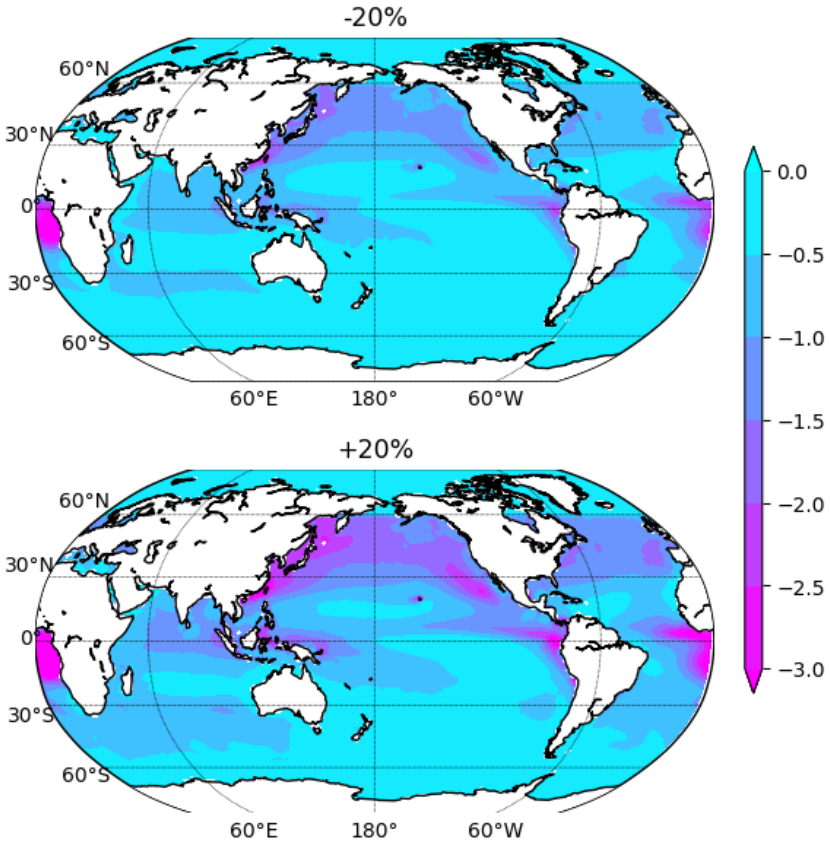

Figure S7 Sensitivity tests with 20% uncertainty in the estimated ΔlnN_d: We adopt the data from Toll et al. (*10*) to get ΔlnN_d and currently have no estimate on its uncertainty range. Here we change the ΔlnN_d by 20% to illustrate the sensitivity of the absolute magnitude of the Twomey effect to a 20% uncertainty. The global mean values are -0.6 and -0.89 Wm^{-2} for the upper and lower panels, respectively. Both is within the current estimate of the Twomey effect (*3*).